Propulsion and Power Research 2018;7(2):182–195

HOSTED BY

ELSEVIER

http://ppr.buaa.edu.cn/

Propulsion and Power Research

www.sciencedirect.com

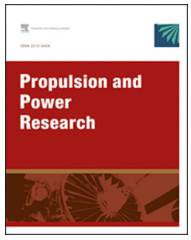

ORIGINAL ARTICLE

Effects of velocity and thermal wall slip on magnetohydrodynamics (MHD) boundary layer viscous flow and heat transfer of a nanofluid over a non-linearly-stretching sheet: a numerical study

Dodda Ramya[a,*], R. Srinivasa Raju[b], J. Anand Rao[a], A.J. Chamkha[c]

[a]*Department of Mathematics, University College of Science, Osmania University, Hyderabad 500007, Telangana State, India*
[b]*Department of Engineering Mathematics, GITAM University, Hyderabad Campus, Rudraram 502329, Medak (Dt), Telangana State, India*
[c]*Mechanical Engineering Department, Prince Mohammad Bin Fahd University, P.O. Box 1664, Al-Khobar 31952, Saudi Arabia*

Received 4 November 2015; accepted 4 March 2016
Available online 6 June 2018

KEYWORDS

Magnetogydrodynamics (MHD);
Nanofluid;
Non-linearly stretching sheet;
Velocity slip;
Thermal slip

Abstract In this analysis, the boundary layer viscous flow of nanofluids and heat transfer over a non-linearly-stretching sheet in the presence of a magnetic field is presented. Velocity and thermal slip conditions are considered instead of no slip conditions at the boundary. A similarity transformation set is used to transform the governing partial differential equations into non-linear ordinary differential equations. The reduced equations are solved numerically using the Keller box method. The influence of the governing parameters on the dimensionless velocity, temperature, nanoparticle concentration as well as the skin friction coefficient, Nusselt number, and local Sherwood number are analyzed. It is found that as the velocity slip parameter increases, the velocity profile is decreased and the skin friction and heat transfer decreased while the mass transfer is increased. Increasing the thermal slip parameter causes decreases in the heat and mass transfer rates. The results are presented in both graphical and tabular forms.

*Corresponding author.
E-mail address: ramyadodda@gmail.com (Dodda Ramya).

Peer review under responsibility of National Laboratory for Aeronautics and Astronautics, China.

https://doi.org/10.1016/j.jppr.2018.04.003

Nomenclature

u, v	velocity components in the x- and y-axis, respectively (unit: m/s)
u_w	velocity of the wall along the x-axis (unit: m/s)
x, y	Cartesian coordinates measured along the stretching sheet (unit: m)
$B(x)$	magnetic field strength (unit: $\mathrm{A \cdot m^{-1}}$)
C	nanoparticle concentration (unit: $\mathrm{mol \cdot m^{-3}}$)
C_{fx}	skin-friction coefficient (pascal)
Nu_x	Nusselt number
Sh_x	Sherwood number
C_w	nanoparticle concentration at the stretching surface (unit: $\mathrm{mol \cdot m^{-3}}$)
C_∞	nanoparticle concentration far from the sheet (unit: $\mathrm{mol \cdot m^{-3}}$)
c_p	specific heat capacity at constant pressure (unit: $\mathrm{J \cdot kg^{-1} \cdot K}$)
D_T	Brownian diffusion coefficient
D_B	thermophoresis diffusion coefficient
Ec	Eckert number
c	constant parameter
n	non-linear stretching parameter
f	dimensionless stream function
Le	Lewis number
M	magnetic parameter
Nb	Brownian motion parameter
Nt	thermophoresis parameter
Pr	Prandtl number
N_1	velocity slip factor
D_1	thermal slip parameter
T	fluid temperature (unit: K)

Greek symbols

σ	electrical conductivity (unit: $\mathrm{S \cdot m^{-1}}$)
ψ	stream function
η	dimensionless similarity variable
μ	dynamic viscosity of the base fluid (unit: $\mathrm{kg/(m \cdot s)}$)
ν	kinematic viscosity (unit: $\mathrm{m^2 \cdot s^{-1}}$)
ρ_f	density of the fluid (unit: $\mathrm{kg \cdot m^{-3}}$)
$(\rho c)_f$	heat capacity of the base fluid (unit: $\mathrm{kg/(m \cdot s^2)}$)
$(\rho c)_\nu$	heat capacity of the nanoparticle (unit: $\mathrm{kg/(m \cdot s^2)}$)
θ	dimensionless temperature (unit: K)
p	pressure (unit: $\mathrm{N/m^2}$)
ϕ	nanoparticle volume fraction
ϕ_w	nanoparticle volume fraction at wall temperature
ϕ_∞	ambient nanoparticle volume fraction
λ	velocity slip parameter
δ	thermal slip parameter
T_w	temperature at the surface (unit: K)
T_∞	temperature of the fluid far away from the stretching sheet (unit: K)
Re_x	Reynolds number

Subscripts

f	fluid
w	condition on the sheet
q_w	surface heat flux (unit: $\mathrm{W/m^2}$)
q_m	surface mass flux
∞	ambient conditions

1. Introduction

The study of a viscous fluid flow of a stretching surface is an important flow occurring in several engineering processes. These processes are wire drawing, heat-treated materials travelling between a wind-up roll and a feed role or materials manufactured by extrusion, paper and glass fiber production, cooling of metallic sheets or electronic chips, drawing of plastic sheets, crystal growing, and many others. In this way, the final product of desired characteristics depends on the cooling process in the stretching sheet [1]. Sakiadis [2] was initiated the study on axi-symmetric and two-dimensional boundary layer flow problems. Various aspects have been studied by several authors in the past decades. However, all these investigations are restricted to linear stretching of the sheet. It is meant by that the stretching is no need linear. In view of this, Kumaran and Ramanaiah [3] studied flow over a quadratic stretching surface, but only some recent investigations focused on non-linearly and exponentially stretching sheet were showed here. Cortell [4] analyzed the heat transfer and viscous flow and over a non-linear stretching sheet numerically. Hayat et al. [5] analyzed the mixed convection flow over a non-linear stretching sheet of a micropolar fluid by using Homotopy analysis method. Rashidi et al. [6] observed the problem on free convective heat and mass transfer for magnetohydrodynamic fluid flow over a permeable vertical stretching sheet in the presence of the radiation and buoyancy effects using homotopy analysis method. Prasad et al. [7] studied the fluid properties on the magnetohydrodynamics (MHD) flow and heat transfer over a stretching surface by using Keller-box method. Rapits and Perdikis [8] studied viscous flow over a non-linearly stretching sheet in the presence of magnetic field and chemical reaction parameters by using shooting method. The magnetohydrodynamic flow of an electric conducting, visco-elastic fluid past a shrinking sheet was studied by Turkyilmazoglu [9] for two classes, namely second-grade and Walter liquid B fluids. Umar khan et al. [10] investigated the effect of thermo diffusion on stagnation point flow of a nanofluid towards a stretching surface with applied magnetic field with the help of similarity transforms. Uddin et al. [11] investigated magneto-convective boundary layer slip flow along a non-isothermal continuously moving permeable non-linear radiating plate embedded in Darcian porous media using Runge-Kutta-Fehlberg fourth-fifth order numerical method.

Nanofluid is a fluid having nanometer-sized particles, called nanoparticles. These fluids of nanoparticles are engineered colloidal suspensions in a base fluid. The nanoparticles are used in nanofluids and typically made of metals (Cu, Ag), oxides (Al_2O_3), carbides (SiC), Nitrides (AlN, SiN) or Nonmetals (Carbon nanotubes, Graphite) and the base fluid is usually a one of the conductive fluid, such as water, glycol, ethylene, toluene and oil. The choice of base fluid-particle combination depends up on the application for which the nanofluid is intended. They have several engineering and biomedical applications in cancer therapy, cooling and process industries. Major advantages of nanofluids are that they are very stable, have sufficient viscosity, spreading, better wetting and dispersion properties on solid surface even for modest nanoparticle concentrations. Nanoparticles are ranged between 1–100 nm in diameter. Experimental studies have shown that nanofluids generally need only contain up to a 5% nanoparticle volume fraction to ensure effective heat transfer enhancements. Nanofluids offer many diverse advantages in application such as fuel nuclear reactors cell, microelectronics, biomedicine and transportation. The term was coined by Choi [12]. The boundary layer heat transfer from a stretching sheet circular cylinder in a nano fluid was investigated by Gorla et al. [13]. Fakour [14] conducted similar research for a Study of heat transfer and flow of Nano fluid in permeable channel in the presence of magnetic field. Makinde and Aziz [15] investigated the boundary layer fluid flow of past a stretching sheet with a convective boundary conditions in nanofluids with the help of RK method. Mustafa et al. [16] investigated the boundary layer flow of an exponential stretching sheet by using homotopy analysis method for the computation of analytical solutions. Hamad [17] found the similarity solutions of heat transfer and viscous flow of nanofluid over a non-linearly stretching sheet using RK method. The steady boundary layer stagnation-point flow toward a stretching/shrinking sheet and heat transfer of a nanofluid past a non-linearly permeable stretching/shrinking sheet was numerically studied by Bachok et. al. [18] and similar research on boundary layer flow and heat transfer over a non-linearly permeable stretching/ shrinking sheet in a nanofluid was studied by Zaimi et al. [19]. The steady two-dimensional stagnation-point flow over a linearly stretching/shrinking sheet in a viscous and incompressible fluid in the presence of a magnetic field was studied by Fazlina Aman et al. [20]. In this research work, The governing partial differential equations were reduced to non-linear ordinary differential equations by a similarity transformation, before being solved numerically by a shooting method. Uddin et al. [21] presented an analysis of two dimensional MHD free convective, viscous, boundary layer nanofluid flow from a convectively heated permeable vertical surface in presence of chemical reaction. In this research work, the authors were used scaling group of transformations for solving the governing equations with the corresponding the boundary conditions. Uddin et al. [22] studied steady two-dimensional magnetohydrodynamic laminar free convective boundary layer slip flow of an electrically conducting Newtonian nanofluid from a translating stretching/shrinking sheet in a quiescent fluid. Uddin et al. [23] studied two-dimensional, steady, laminar mixed convective boundary-layer slip nanofluid flow in a Darcian porous medium due to a stretching/shrinking sheet in presence of thermal radiation theoretically and numerically. Uddin et al. [24] studied the effect of constant convective thermal and mass boundary conditions of two-dimensional laminar g-jitter mixed convective boundary layer flow of water-based nanofluids. In this research work, the governing transport equations were converted into non-similar equations using suitable transformations, before being solved numerically by an implicit finite difference method with quasi-linearization technique. Rashidi et al. [25] studied the effect of heat transfer on steady, incompressible water based nanofluid flow over a stretching sheet in the presence of transverse magnetic field with thermal radiation and buoyancy effects. In this paper, the authors were used similarity transformation for reducing the governing momentum and energy equations into non-linear ordinary differential equations, and the resulting differential equations with the appropriate boundary conditions were solved by shooting iteration technique together with fourth-order Runge-Kutta integration scheme. Several other studies have addressed in various aspects of nanofluids (including comparison) with stretching sheet [26–31].

The fluid's effect of boundary slip has important applications such as in the polishing of artificial internal cavities and heart valves. Velocity and thermal jump conditions are adequate for the flow of liquids at the micro-scale level especially in this way the lack of data on the thermal digs coefficient. Among the application of several complex micro-channels and micro-devices arise. For instance, the micro-conducts of rectangular, trapezoidal and triangular sections crossing are very familiar and easy to make in the micro-scale thermal fluid system. Mustafa et al. [32] studied the slip effects of nanofluid in a channel with wall properties on the peristaltic motion by using homotopy analysis method (HAM). Recently, the combined effects of velocity slip and thermal slip on unsteady stagnation point flow of a nanofluid over a stretching sheet were investigated numerically by Malvandi et al. [33]. Umar Khan [34] Investigated effects of viscous dissipation and slip velocity on two-dimensional and axisymmetric squeezing flow of cu-water and cu-kerosene nano fluids. Turkyilmazoglu [35] presented an analysis of magnetohydrodynamic flow and heat transfer over permeable stretching/shrinking surface taking into account a second order slip. In this paper, the author found analytical solutions for the flow and heat valid under various physical conditions. Turkyilmazoglu [36] found on dual and triple solutions for MHD slip flow an electrically conducting, non-Newtonian fluid past a shrinking sheet under the influence of slip flow conditions. The correspondence between certain nanofluids and standard fluid flow was studied by Turkyilmazoglu [37] by introducing a rescaling approach that greatly simplifying the

evaluation of flow and physical parameters such as skin friction and heat transfer rate. Turkyilmazoglu [38] studied the nanoparticles across the condensate boundary layer which was the most used model (single phase) and the concentration of nanoparticles through the film was allowed to vary from the wall to the outer edge of the condensate film in the light of modified Buongiorno's nanofluid model (multi-phase). In this paper the author solved momentum and energy equations analytically in both theoretical cases to deduce the flow and heat transport phenomena. The homotopy analysis method was employed by Rashidi et al. [39] for examining free convective heat and mass transfer in a steady two-dimensional magnetohydrodynamic fluid flow over a stretching vertical surface in porous medium. Rashidi and Erfani [40] studied the combined effects of thermal-diffusion and diffusion-thermo on steady MHD convective and slip flow due to a rotating disk with viscous dissipation and Ohmic heating in presence of heat and mass transfer. Abbasbandy et al. [41] found both the numerical and analytical solutions for Falkner-Skan flow of magnetohydrodynamic Oldroyd-B fluid using homotopy analysis method and numerical Keller box method.

To the best of authors' knowledge, there is not any investigation to address the slip effects of viscous flow of nanofluids and heat transfer over a non-linearly stretching sheet in the presence of a magnetic field effect. The aim of the present study is to extend the work of Hamad [17]. The boundary layer flow and heat transfer of a nanofluid which exhibits wall slip conditions is considered and the governing partial equations are transformed into ordinary differential equations and solved numerically by using the Keller-box method.

2. Formulation of the problem

Consider steady, two-dimensional and incompressible viscous laminar flow of an electrically-conducting fluid over a non-linearly stretching surface (Figure 1). The sheet is extended with a velocity $u_w = ax^n$ with fixed origin location, where n is a non-linear stretching parameter, a is a constant and x is the coordinate measured along the stretching surface. The flow takes place at $y \geq 0$ where y is the coordinate measured to the stretching sheet, a steady uniform stress leading to equal and opposite forces is applied along the x-axis, the sheet is stretched keeping the origin fixed. The wall temperature T_w and the nanoparticle fraction C_w are assumed constant at the stretching surface while the ambient temperature and nanoparticle fraction have constant values T_∞ and C_∞, respectively. In addition, velocity slip and thermal slip conditions are taken into account at the wall and the effect of the magnetic field is incorporated through the momentum equation [17]. Under the above assumptions, the governing continuity, momentum and thermal energy and nanoparticles equation of the nanofluid can be written in vector form using Cartesian coordinates x and y as [42].

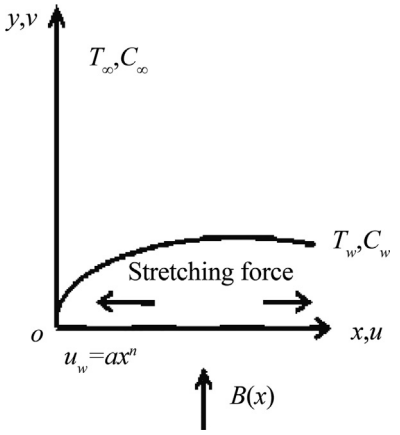

Figure 1 Physical model and coordinate system.

$$\nabla \cdot V = 0 \tag{1}$$

$$\rho_f \left(\frac{\partial V}{\partial t} + V \cdot \nabla V \right) = -\nabla P + \mu \nabla^2 V - \sigma B^2 (\nabla \cdot V) \tag{2}$$

$$(\rho c)_f \left(\frac{\partial T}{\partial t} + V \cdot \nabla T \right) = K \nabla^2 T + (\rho c)_p \left[D_B \nabla C \cdot \nabla T + \left(\frac{D_T}{T_\infty} \right) \nabla T \cdot \nabla T \right] \tag{3}$$

$$\left(\frac{\partial C}{\partial t} + V \cdot \nabla C \right) = \left[D_B \nabla^2 C + \left(\frac{D_T}{T_\infty} \right) \nabla^2 T \right] \tag{4}$$

Here we write V is a function of u and v. We now make the standard boundary-layer approximation, based on a scale analysis, and write the governing equations [43]:

$$\frac{\partial u}{\partial x} + \frac{\partial v}{\partial y} = 0 \tag{5}$$

$$u \frac{\partial u}{\partial x} + v \frac{\partial u}{\partial y} = \nu \frac{\partial^2 u}{\partial y^2} - \frac{\sigma B^2}{\rho_f} u \tag{6}$$

$$u \frac{\partial T}{\partial x} + v \frac{\partial T}{\partial y} = \alpha \frac{\partial^2 T}{\partial y^2} + \frac{\nu}{c_p} \left(\frac{\partial u}{\partial y} \right)^2 + \tau \left\{ D_B \frac{\partial T}{\partial y} \frac{\partial C}{\partial y} + \frac{D_T}{T_\infty} \left(\frac{\partial T}{\partial y} \right)^2 \right\} \tag{7}$$

$$u \frac{\partial C}{\partial x} + v \frac{\partial C}{\partial y} = D_B \frac{\partial^2 C}{\partial y^2} + \frac{D_T}{T_\infty} \left(\frac{\partial^2 T}{\partial y^2} \right) \tag{8}$$

Where $\alpha = \frac{K}{(\rho c)_f} \left(\mathrm{m}^2/\mathrm{s} \right)$ is the thermal diffusivity, and $\tau = \frac{(\rho c)_p}{(\rho c)_f}$ is the ratio between the effective heat capacity of the fluid. We assume that the variable magnetic field $B(x) = B_0 x^{n-1/2}$. This form of $B(x)$ has also been considered many authors.

2.1. Boundary conditions

The appropriate boundary conditions [44] for the problem are given by

$$\left.\begin{aligned} &u = u_w + N v_f\left(\frac{\partial u}{\partial y}\right),\ v = 0,\\ &T = T_w + D\left(\frac{\partial T}{\partial y}\right),\ C = C_w \text{ as } y = 0\\ &u \to 0,\ v \to 0,\ T = T_\infty,\ C = C_\infty \text{ as } y \to \infty \end{aligned}\right\} \tag{9}$$

Here $u_w = cx^n$ is the stretching velocity, $T_w = T_\infty + bx^{2n}$ is the temperature at the sheet, c, b are constants is the non-linear stretching parameter, $N = N_1 x^{\frac{-n-1}{2}}$ is the velocity slip factor which changes with x, and N_1 is the initial value of velocity slip factor and $D = D_1 x^{\frac{-n-1}{2}}$ is the thermal slip factor which changes with x, and D_1 is the initial value of thermal slip, no-slip case is recovered for $N = 0 = D$.

Introducing the similarity variables as

$$\left.\begin{aligned} &\eta = y\sqrt{a(n+1)/2\nu_f}\,x^{(n-1)/2},\\ &u = ax^n f'(\eta),\\ &v = -\sqrt{\frac{(n+1)a\nu_f}{2}}\,x^{n-1/2}[f(\eta) + \tfrac{n-1}{n+1}\eta f'(\eta)],\\ &T = T_\infty + bx^{2n}\theta(\eta),\ \varphi(\eta) = (C - C_\infty)/(C_w - C_\infty) \end{aligned}\right\} \tag{10}$$

Using Eq. (9), Eqs. (5)–(8) become

$$f''' + ff'' - \left(\frac{2n}{n+1}\right)f'^2 - Mf' = 0 \tag{11}$$

$$\frac{1}{Pr}\theta'' + f\theta' - \left(\frac{4n}{n+1}\right)f'\theta + Nb\theta'\varphi' + Nt\theta'^2 + Ecf''^2 = 0 \tag{12}$$

$$\phi'' + Lef\phi' + \frac{Nt}{Nb}\theta'' = 0 \tag{13}$$

and the corresponding boundary conditions (9) become

$$\left.\begin{aligned} &f' = 1 + \lambda f''(0),\ f = 0,\\ &\theta = 1 + \delta\theta'(0),\ \varphi = 1 \text{ at } \eta = 0\\ &f' \to 0,\ \theta \to 0,\ \varphi \to 0 \text{ as } \eta \to \infty \end{aligned}\right\} \tag{14}$$

where primes denote differentiation with respect to η.

The involved physical parameters are defined as

$$\left.\begin{aligned} &Pr = \tfrac{\nu}{\alpha},\ Le = \tfrac{\alpha}{D_B},\ Nb = \tfrac{(\rho c)_f D_B (C_w - C_\infty)}{(\rho c)_f \alpha},\\ &Nt = \tfrac{(\rho c)_f D_T (T_w - T_\infty)}{(\rho c)_f T_\infty \alpha},\ M = \tfrac{2\sigma B_o^2}{c\rho_f(n+1)},\\ &\lambda = N_1\sqrt{\tfrac{a\nu_f(n+1)}{2}},\ \delta = D_1\sqrt{\tfrac{a(n+1)}{2\nu_f}},\\ &Ec = \tfrac{u_w^2}{c_p(T_w - T_\infty)} \end{aligned}\right\} \tag{15}$$

The quantities of the practical interest, in this study, are the local skin friction

$$\left.\begin{aligned} &C_{fx} = \tfrac{\mu_f}{\rho u_w^2}\left[\tfrac{\partial u}{\partial y}\right]_{y=0},\\ &Nu_x = \tfrac{xq_w}{k(T_w - T_\infty)},\\ &Sh_x = \tfrac{xq_m}{D_B(C_w - C_\infty)} \end{aligned}\right\} \tag{16}$$

where k is the thermal conductivity of the nanofluid, and q_w, q_m are the heat and mass fluxes at the surface, given by

$$q_w = -\left[\frac{\partial T}{\partial y}\right]_{y=0},\ q_m = -D_B\left[\frac{\partial C}{\partial y}\right]_{y=0} \tag{17}$$

Substituting Eq. (9) into Eqs. (11)–(13), we obtain

$$\left.\begin{aligned} &Re_x^{1/2} Cf_x = \sqrt{\tfrac{n+1}{2}}f''(0),\\ &Re_x^{-1/2} Nu_x = -\sqrt{\tfrac{n+1}{2}}\theta'(0),\\ &Re_x^{1/2} Sh_x = -\sqrt{\tfrac{n+1}{2}}\varphi'(0) \end{aligned}\right\} \tag{18}$$

where $Re_x = u_w x/\nu$ is the local Reynolds number.

3. Solution of the problem by Keller-box method

As Eqs. (11)–(13) are non-linear, it is impossible to get closed-form solutions. Consequently, the equations with the boundary conditions (14) are solved numerically by means of a finite-difference scheme known as the Keller-box method. Keller [45] developed the scheme. This method has been shown to be particularly accurate for parabolic problems It is much easier and faster to program and it is chosen because it seems to be the most flexible of the common methods, we have used the procedure outlined in Cebeci and Pradshaw [46], which has been found to be very suitable in dealing with non-linear problems easily adaptable to solving equations of any order. The principal steps in the Keller box method is to get the numerical solutions are the following:

i. Transform the given first-order equations of ODEs to a system.
ii. Write the reduced ODEs in finite differences.
iii. By using Newton's method, linearized the algebraic equations and write them in a vector form.
iv. Solve the linear system by the block tri-diagonal elimination technique.

3.1. Solution procedure

3.1.1. Finite difference method

To solve the transformed differential Eqs. (11)–(13) subjected to the boundary conditions (14), Eqs. (11)–(13) are first converted into a system of seven first-order equations, and the difference equations are then expressed using central differences. For this purpose, we introduce new dependent variables $p(\eta)$, $q(\eta)$, $\theta(\eta)$, $t(\eta)$, $\phi(\eta)$ and $v(\eta)$ so that Eqs. (11)–(13) can be written as

$$f' = p \tag{19}$$

$$p' = q \tag{20}$$

$$\theta' = t \tag{21}$$

$$\phi' = v \tag{22}$$

$$q' + fq - \left(\frac{2n}{n+1}\right)p^2 - Mp = 0 \tag{23}$$

$$\tfrac{1}{Pr}t' + ft - \left(\tfrac{4n}{n+1}\right)p\theta + Nb(tv) + Nt\left(t^2\right) + Ec\left(q^2\right) = 0 \tag{24}$$

$$v' + Le(fv) + \left(\frac{Nt}{Nb}\right)t' = 0 \tag{25}$$

In terms of the new dependent variables, the boundary conditions (14) are given by

$$\left.\begin{array}{l} p(0) = 1 + \lambda q(0), \;\; \varphi(0) = 1 \\ f(0) = 0, \;\; \theta(0) = 1 + \delta t(0), \\ p(\eta) \to 0, \;\; \theta(\eta) \to 0, \;\; \varphi(\eta) \to 0 \;\text{ as }\; \eta \to \infty \end{array}\right\} \tag{26}$$

We now consider the segment $\eta_{j-1}\eta_j$ with $\eta_{j-1/2}$ as the midpoint, which is defined as below:

$$\eta_0 = 0, \; \eta_j = \eta_{j-1} + h_j, \; \eta_j = \eta_\infty \tag{27}$$

Where h_j is the $\Delta\eta$-spacing and $\Delta\eta = 1,2,\ldots,J$ is a sequence number that indicates the coordinate location. The finite difference approximations (11)–(17) written for the midpoint $\eta_{j-1/2}$ and arranging the expression

$$f_j - f_{j-1} - \frac{1}{2}h_j\left(p_j + p_{j-1}\right) = 0 \tag{28}$$

$$p_j - p_{j-1} - \frac{1}{2}h_j\left(q_j + q_{j-1}\right) = 0 \tag{29}$$

$$\theta_j - \theta_{j-1} - \frac{1}{2}h_j\left(t_j + t_{j-1}\right) = 0 \tag{30}$$

$$\phi_j - \phi_{j-1} - \frac{1}{2}h_j\left(\nu_j + \nu_{j-1}\right) = 0 \tag{31}$$

$$q_j - q_{j-1} - \frac{1}{2}h_j(fq)_{j-1/2} - h_j\left(\frac{2n}{n+1}\right)\left(p^2_{j-1}\right) - Mp_{j-1/2} = 0 \tag{32}$$

$$\frac{1}{Pr}\left(t_j - t_{j-1}\right) + h_j(ft)_{j-1/2} - h_j\left(\frac{4n}{n+1}\right)(p\theta)_{j-1/2} + h_jNb(tv)_{j-1/2} + h_jNt\left(t^2_{j-1/2}\right) + h_jEc\left(q^2_{j-1/2}\right) = 0 \tag{33}$$

$$v_j - v_{j-1} + Leh_j(fv)_{j-1/2} + \frac{Nt}{Nb}\left(t_j - t_{j-1}\right) = 0 \tag{34}$$

Eqs. (27)–(33) are imposed for $j = 1,2,\ldots,J$, and the transformed boundary layer thickness η_J is to be sufficiently large so that it is beyond the edge of the boundary layer.

The boundary conditions are

$$\left.\begin{array}{l} f_0 = 0, \; p_0 = 1 + \lambda q(0), \; \theta_0 = 1 + \delta t(0), \\ \varphi_0 = 1, \;\; p_J = 0, \;\; \theta_J = 0, \;\; \varphi_J = 0 \end{array}\right\} \tag{35}$$

3.1.2. Newton's method

To, linearized the non-linear system (28)–(34), We use Newton's method, by introducing the following expressions:

$$\left.\begin{array}{l} f_j^{(k+1)} = f_j^{(k)} + \delta f_j^{(k)}, \; p_j^{(k+1)} = p_j^{(k)} + \delta p_j^{(k)}, \\ q_j^{(k+1)} = q_j^{(k)} + \delta q_j^{(k)}, \; \theta_j^{(k+1)} = \theta_j^{(k)} + \delta\theta_j^{(k)}, \\ t_j^{(k+1)} = t_j^{(k)} + \delta t_j^{(k)}, \; \phi_j^{(k+1)} = \phi_j^{(k)} + \delta\phi_j^{(k)}, \\ v_j^{(k+1)} = v_j^{(k)} + \delta v_j^{(k)} \end{array}\right\} \tag{36}$$

Where $k = 0,1,2,3,\ldots.$

We then insert the left-hand side expressions in place of $\delta p^{(k)}$, $\delta q^{(k)}$, $\delta\theta^{(k)}$, $\delta t^{(k)}$, $\delta\phi^{(k)}$ and $\delta v^{(k)}$.

This procedure yields the following linear system (the superscript k is dropped for simplicity):

$$\delta f_j - \delta f_{j-1} - \frac{h_j}{2}(\delta p_j + \delta p_{j-1}) = (r_1)_{j-1/2} \tag{37}$$

$$\delta p_j - \delta p_{j-1} - \frac{h_j}{2}(\delta q_j + \delta q_{j-1}) = (r_2)_{j-1/2}, \tag{38}$$

$$\delta\theta_j - \delta\theta_{j-1} - \frac{h_j}{2}(\delta t_j + \delta t_{j-1}) = (r_3)_{j-1/2}, \tag{39}$$

$$\delta\phi_j - \delta\phi_{j-1} - \frac{h_j}{2}(\delta v_j + \delta v_{j-1}) = (r_4)_{j-1/2}, \tag{40}$$

$$(a_1)\delta q_j + (a_2)\delta q_{j-1} + (a_3)\delta f_j + (a_4)\delta f_j + (a_5)\delta p_j + (a_6)\delta p_{j-1} = (r_5)_{j-1/2} \tag{41}$$

$$(b_1)\delta t_j + (b_2)\delta t_{j-1} + (b_3)\delta f_j + (b_4)\delta f_j + (b_5)\delta p_j + (b_6)\delta p_{j-1} + (b_7)\delta\theta_j + (b_8)\delta\theta_{j-1} + (b_9)\delta t_j + (b_{10})\delta t_{j-1} + (b_{11})\delta q_j + (b_{12})\delta q_{j-1} = (r_6)_{j-1/2} \tag{42}$$

$$(c_1)\delta v_j + (c_2)\delta v_{j-1} + (c_3)\delta f_j + (c_4)\delta f_j + (c_5)\delta t_j + (c_6)\delta t_{j-1} = (r_7)_{j-1/2} \tag{43}$$

where

$$\left.\begin{array}{l} (a_1)_j = 1 + \frac{h_j}{2}f_{j-1/2}, \\ (a_2)_j = (a_1)_j - 2, \\ (a_3)_j = \frac{h_j}{2}q_{j-1/2}, \\ (a_4)_j = (a_3)_j, \\ (a_5)_j = -\frac{2n}{n+1}h_jp_{j-1/2} - \frac{M}{2}h_j, \\ (a_6)_j = (a_5)_j, \end{array}\right\} \tag{44}$$

$$\left.\begin{aligned}
(b_1)_j &= \tfrac{1}{pr} + \tfrac{h_j}{2} f_{j-1/2} + Nb \cdot \tfrac{h_j}{2} \nu_{j-1/2} + Nt \cdot h_j t_{j-1/2},\\
(b_2)_j &= (b_2)_j - \tfrac{2}{pr},\\
(b_3)_j &= \tfrac{h_j}{2} t_{j-1/2},\\
(b_4)_j &= (b_3)_j,\\
(b_5)_j &= -\tfrac{h_j}{2} \cdot \tfrac{4n}{n+1} \cdot p_{j-1/2},\\
(b_6)_j &= (b_5)_j,\\
(b_7)_j &= -\tfrac{h_j}{2} \cdot \tfrac{4n}{n+1} \cdot \theta_{j-1/2},\\
(b_8)_j &= (b_7)_j\\
(b_9)_j &= \tfrac{h_j}{2} t_{j-1/2} \cdot Nb,\\
(b_{10})_j &= (b_9)_j,\\
(b_{11})_j &= Ec \cdot \tfrac{h_j}{2} q_{j-1/2},\\
(b_{12})_j &= (b_{11})_j,
\end{aligned}\right\} \tag{45}$$

$$\left.\begin{aligned}
(c_1)_j &= 1 + \tfrac{h_j}{2} Le \cdot f_{j-1/2},\\
(c_2)_j &= (c_1)_j - 2,\\
(c_3)_j &= Le \cdot \tfrac{h_j}{2} \nu_{j-1/2},\\
(c_5)_j &= \tfrac{Nt}{Nb},\\
(c_6)_j &= -(c_5)_j,
\end{aligned}\right\} \tag{46}$$

$$\left.\begin{aligned}
(r_1) &= f_{j-1} - f_j + h_j (p_{j-\frac{1}{2}}),\\
(r_2) &= p_{j-1} - p_j + h_j (q_{j-\frac{1}{2}}),\\
(r_3) &= \theta_{j-1} - \theta_j + h_j (t_{j-\frac{1}{2}}),\\
(r_4) &= \phi_{j-1} - \phi_j + h_j (\nu_{j-\frac{1}{2}}),\\
(r_5) &= q_{j-1} - q_j - h_j (fq)_{j-\frac{1}{2}} + \tfrac{2n}{n+1} p^2_{j-1/2} - (M) p_j,\\
(r_6) &= \tfrac{1}{pr} (t_{j-1} - t_j) - h_j (Nb \cdot (vt)_{j-\frac{1}{2}} - Nt \cdot t^2_{j-\frac{1}{2}} -\\
& Ec \cdot q^2_{j-\frac{1}{2}} - \tfrac{4n}{n+1} (p\theta)_{j-\frac{1}{2}} + (ft)_{j-\frac{1}{2}})\\
(r_7) &= \nu_j - \nu_{j-1} - h_j (Le \cdot (fv)_{j-\frac{1}{2}}) - \tfrac{Nt}{Nb} (t_j - t_{j-1}),
\end{aligned}\right\} \tag{47}$$

The boundary conditions (34) become

$$\begin{aligned}
&\delta f_0 = 0,\ \delta p_0 = 0,\ \delta q_0 = 0,\ \delta \theta_0 = 0,\ \delta \phi_0 = 0,\\
&\delta p_j = 0,\ \delta \theta_j = 0,\ \delta \phi_j = 0
\end{aligned} \tag{48}$$

which just express the requirement for the boundary conditions to remain constant during the iteration process.

3.1.3. *Block-elimination method*

The linearized difference Eqs. (42)–(48) can be solved by the block-elimination method as outlined by Cebeci and Bradshaw [46], since the system has block-tridiagonal structure. Commonly, the block-tridiagonal structure consists of variables or constants, but here an interesting feature can be observed that it consists of block matrices. In a matrix-vector form, Eqs. (42)–(48) can be written as

$$A\boldsymbol{\delta} = \boldsymbol{r} \tag{49}$$

Where

$$\boldsymbol{A} = \begin{bmatrix}
[A_1] & [C_1] & & & & & \\
[B_2] & [A_2] & [C_2] & & & & \\
 & \ddots & \ddots & \ddots & & & \\
 & & & [B_{j-1}] & [A_{j-1}] & [C_{j-1}] & \\
 & & & & [B_j] & [A_j] &
\end{bmatrix} \tag{50}$$

$$\boldsymbol{\delta} = \begin{bmatrix} [\delta_1] \\ [\delta_2] \\ \vdots \\ [\delta_{j-1}] \\ [\delta_j] \end{bmatrix} \text{ and } \boldsymbol{r} = \begin{bmatrix} [r_1] \\ [r_2] \\ \vdots \\ [r_{j-1}] \\ [r_j] \end{bmatrix} \tag{51}$$

The elements of the matrices are as follows:

$$[A_1] = \begin{bmatrix}
0 & 0 & 0 & 1 & 0 & 0 & 0 \\
-\frac{h_j}{2} & 0 & 0 & 0 & -\frac{h_j}{2} & 0 & 0 \\
0 & -\frac{h_j}{2} & 0 & 0 & 0 & -\frac{h_j}{2} & 0 \\
0 & 0 & -\frac{h_j}{2} & 0 & 0 & 0 & -\frac{h_j}{2} \\
(a_2)_1 & 0 & 0 & (a_3)_1 & (a_1)_1 & 0 & 0 \\
(b_{12})_1 & (b_2)_1 & (b_{10})_1 & (b_3)_1 & (b_{11})_1 & (b_1)_1 & (b_9)_1 \\
0 & (c_6)_1 & (c_2)_1 & (c_3)_1 & 0 & (c_5)_1 & (c_1)_1
\end{bmatrix} \tag{52}$$

$2 \le j \le J$:

$$[A_J] = \begin{bmatrix}
-\frac{h_j}{2} & 0 & 0 & 1 & 0 & 0 & 0 \\
-1 & 0 & 0 & 0 & -\frac{h_j}{2} & 0 & 0 \\
0 & -1 & 0 & 0 & 0 & -\frac{h_j}{2} & 0 \\
0 & 0 & -1 & 0 & 0 & 0 & -\frac{h_j}{2} \\
(a_6)_J & 0 & 0 & (a_3)_J & (a_1)_J & 0 & 0 \\
(b_8)_J & (b_6)_J & 0 & (b_3)_J & (b_{11})_J & (b_1)_J & 0 \\
0 & 0 & 0 & (c_3)_J & 0 & (c_5)_J & (c_1)_J
\end{bmatrix} \tag{53}$$

$$[B_j] = \begin{bmatrix}
0 & 0 & 0 & -1 & 0 & 0 & 0 \\
0 & 0 & 0 & 0 & -\frac{h_j}{2} & 0 & 0 \\
0 & 0 & 0 & 0 & 0 & -\frac{h_j}{2} & 0 \\
0 & 0 & 0 & 0 & 0 & 0 & -\frac{h_j}{2} \\
0 & 0 & 0 & (a_4)_J & (a_2)_J & 0 & 0 \\
0 & 0 & 0 & (b_4)_J & (b_{12})_J & (b_2)_J & (b_{10})_J \\
0 & 0 & 0 & (c_4)_J & 0 & (c_6)_J & (c_2)_J
\end{bmatrix} \tag{54}$$

$1 \le j \le J\text{-}1$:

$$[C_J] = \begin{bmatrix} -\frac{h_j}{2} & 0 & 0 & 0 & 0 & 0 & 0 \\ 1 & 0 & 0 & 0 & 0 & 0 & 0 \\ 0 & 1 & 0 & 0 & 0 & 0 & 0 \\ 0 & 0 & 1 & 0 & 0 & 0 & 0 \\ (a_5)_J & 0 & 0 & 0 & 0 & 0 & 0 \\ (b_7)_J & 0 & 0 & 0 & 0 & 0 & 0 \\ 0 & 0 & 0 & 0 & 0 & 0 & 0 \end{bmatrix} \tag{55}$$

$2 \le j \le J$:

$$[\delta_1] = \begin{bmatrix} \delta q_0 \\ \delta\theta_0 \\ \delta\phi_0 \\ \delta f_1 \\ \delta q_1 \\ \delta t_1 \\ \delta v_1 \end{bmatrix}, \quad [\delta_j] = \begin{bmatrix} \delta q_{j-1} \\ \delta\theta_{j-1} \\ \delta\phi_{j-1} \\ \delta f_j \\ \delta q_j \\ \delta t_j \\ \delta v_j \end{bmatrix} \tag{56}$$

$1 \le j \le J$:

$$[r_j] = \begin{bmatrix} (r_1)_{j-1/2} \\ (r_2)_{j-1/2} \\ (r_3)_{j-1/2} \\ (r_4)_{j-1/2} \\ (r_5)_{j-1/2} \\ (r_6)_{j-1/2} \\ (r_7)_{j-1/2} \end{bmatrix} \tag{57}$$

We assume that $\boldsymbol{A}$ is non-singular and it can be factorized as

$$\boldsymbol{A} = \boldsymbol{LU} \tag{58}$$

Where

$$\boldsymbol{L} = \begin{bmatrix} [\alpha_1] & & & & & \\ [\beta_2] & [\alpha_2] & [c_2] & & & \\ & & \ddots & & & \\ & & \ddots & & & \\ & & & & [\alpha_{j-1}] & \\ & & & & [B_j] & [\alpha_j] \end{bmatrix} \tag{59}$$

And

$$\boldsymbol{U} = \begin{bmatrix} [I_1] & [\Gamma_{j-1}] & & & & \\ & [I_1] & & & & \\ & & \ddots & & & \\ & & \ddots & & & \\ & & & & [I_{j-1}] & [\Gamma_{j-1}] \\ & & & & & [I] \end{bmatrix} \tag{60}$$

Where $[I]$ is a 7×7 identity matrix, while $[\alpha_i]$ and $[\Gamma_i]$ are 7×7 matrices in which elements are determined by the following equations:

$$[\alpha_i] = [A_1] \tag{61}$$

$$[A_1][\Gamma_1] = [C_1] \tag{62}$$

$$[\alpha_i] = [A_1] - [B_j][\Gamma_{j-1}], j = 2, 3, \ldots, J \tag{63}$$

$$[\alpha_j][\Gamma_j] = [C_j], j = 2, 3, \ldots, J-1 \tag{64}$$

Substituting Eq. (61) into Eq. (49), we obtain

$$\boldsymbol{LU\delta} = \boldsymbol{r} \tag{65}$$

If we define

$$U\boldsymbol{\delta} = \boldsymbol{W} \tag{66}$$

Then Eq. (66) becomes

$$\boldsymbol{LW} = \boldsymbol{r} \tag{67}$$

Where

$$\boldsymbol{W} = \begin{bmatrix} [W_1] \\ [W_2] \\ \vdots \\ [W_{j-1}] \\ [W_j] \end{bmatrix} \tag{68}$$

The elements of $\boldsymbol{W}$ can be determined from Eq. (68) by the following relations:

$$[\alpha_1][W_1] = [r_1], \quad [\alpha_i][W_j] = [r_j] - [B_i][W_{j-1}], \quad 2 \le j \le J \tag{69}$$

When the elements of $\boldsymbol{W}$ have been found, Eq. (69) gives the solution for $\boldsymbol{\delta}$ in which the elements are found from the following relations:

$$[\delta_J] = [W_J], \quad [\delta_i] = [W_J] - [\Gamma_j][\delta_{j+1}], \quad 1 \le j \le J-1 \tag{70}$$

These calculations are repeated until some convergence criterion is satisfied and calculations are stopped when

$$|\delta v_0| \le \varepsilon_1 \tag{71}$$

where ε_1 is small prescribed value. One of the factors that are affecting the accuracy of the method is the appropriateness of the initial guesses. The accuracy of the method depends on the choice of the initial guesses. The choices of the initial guesses depend on the convergence criteria and the boundary conditions (14).

The following initial guesses are chosen

$$\left.\begin{aligned} f_0(\eta) &= (1/(1+\lambda)) - (1/(1+\lambda))e^{-\eta}, \\ g_0(\eta) &= (1/(1+\delta))e^{-\eta}, \quad h_0(\eta) = e^{-\eta} \end{aligned}\right\} \tag{72}$$

In this study, a uniform grid of size $\Delta\eta = 0.006$ is found to be satisfy the convergence and the solutions are obtained with an error of tolerance 10^{-5} in all cases. In our study, this gives about four decimal places accurate to most of the prescribed quantities.

4. Results and discussion

In order to study the results, a numerical computation effort has been carried out using the method described in the previous section for several values of the velocity slip parameter (λ), thermal slip parameter (δ), magnetic parameter (M). The result of the parametric study are plotted in Figures 2–17. For the verification of the accuracy of the applied numerical scheme, equivalence of the present results corresponding to the values of heat transfer coefficient $[-\theta'(0)]$, mass transfer coefficient $\phi'(0)$ for $M = 0$, $\lambda = 0$, $\delta = 0$ (i.e. in absence of velocity slip, thermal slip and magnetic parameters) are made with the available results of Hamad et al. [17] presented in Tables 1 and 2. The calculation for skin friction coefficient, heat transfer rate

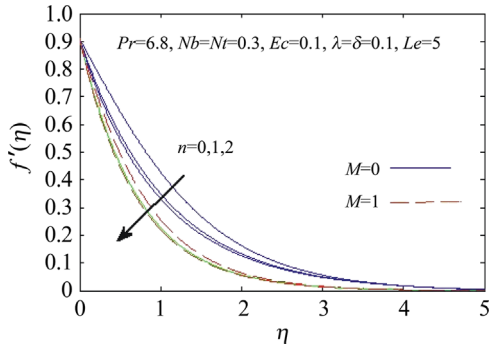

Figure 2 Variation of velocity $f'(\eta)$ with η for several values of M and n.

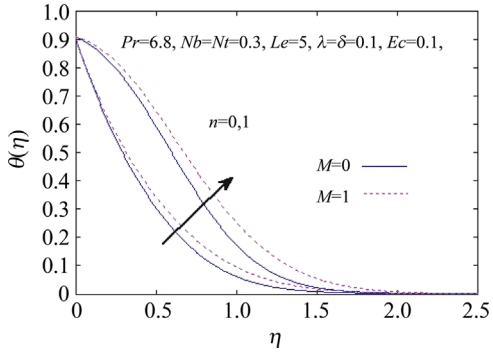

Figure 3 Variation of temperature $\theta(\eta)$ with η for several values of M and n.

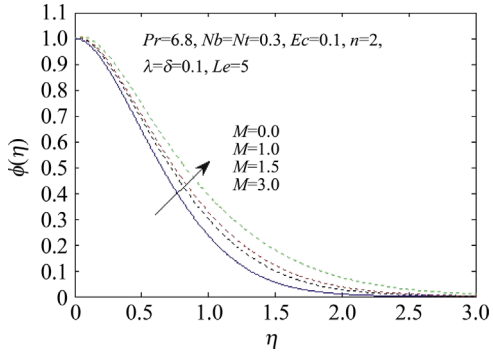

Figure 4 Variation of velocity $\phi(\eta)$ with η for several values of M.

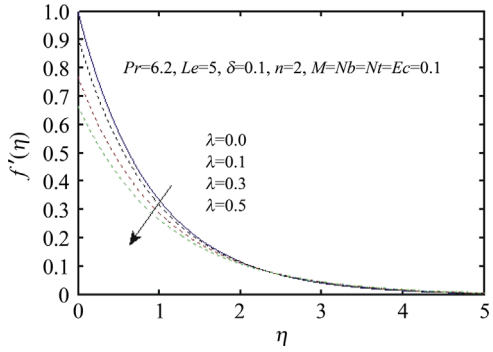

Figure 5 Variation of concentration $f'(\eta)$ with η for several values of λ.

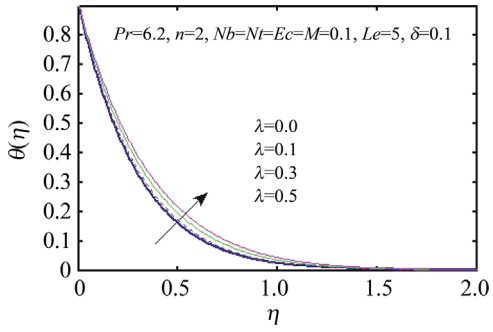

Figure 6 Variation of temperature $\theta(\eta)$ with η for several values of velocity slip parameter λ.

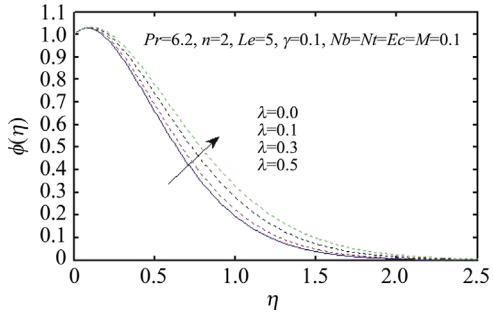

Figure 7 Variation of concentration $\phi(\eta)$ with η for several values of velocity slip parameter λ.

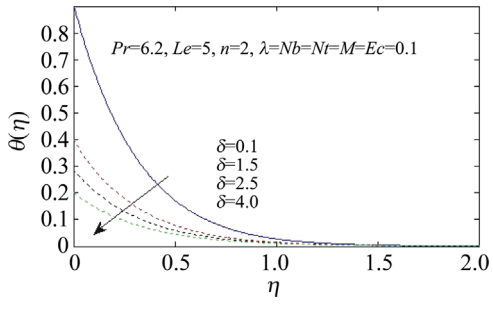

Figure 8 Variation of temperature $\theta(\eta)$ with η for several values of thermal slip parameter δ.

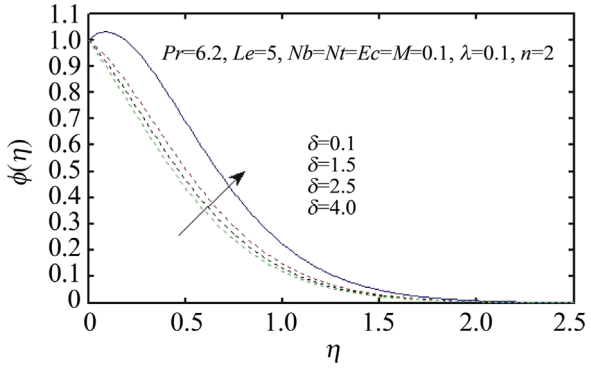

Figure 9 Variation of concentration $\phi(\eta)$ with η for several values of thermal slip parameter δ.

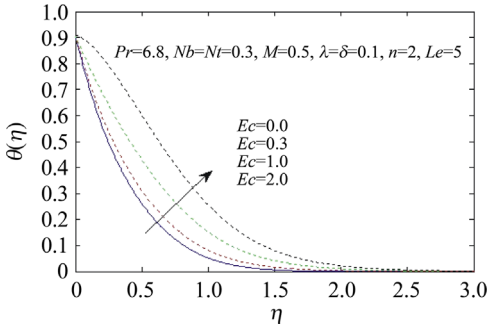

Figure 10 Effect of *Ec* on temperature distribution.

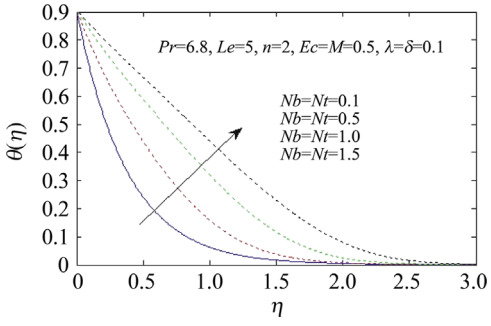

Figure 11 Effects of *Nb* and *Nt* on temperature distribution.

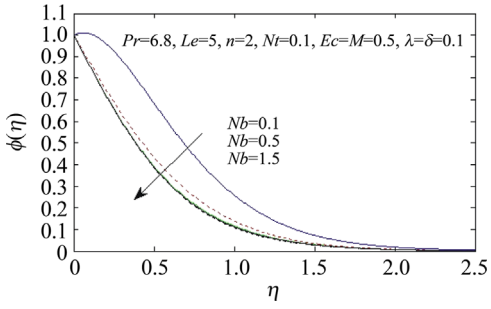

Figure 12 Effect of *Nb* on concentration.

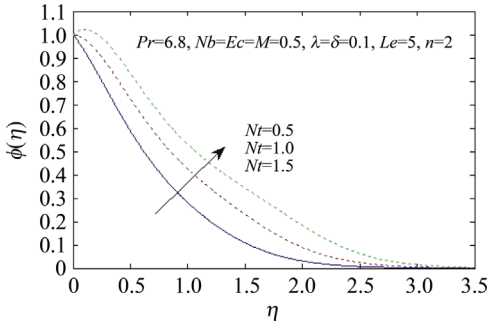

Figure 13 Effect of *Nt* on concentration.

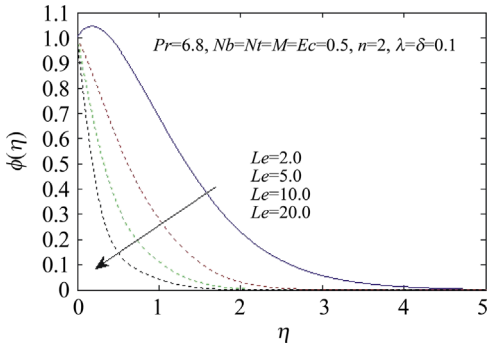

Figure 14 Effect of *Le* on concentration.

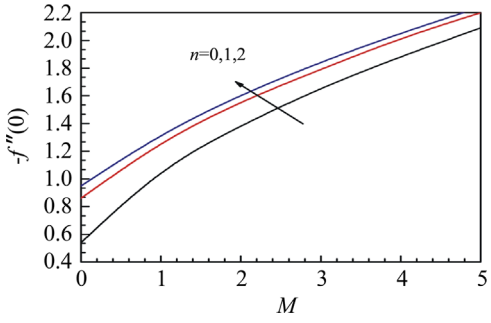

Figure 15 Effects of *M* and *n* on skin friction coefficient.

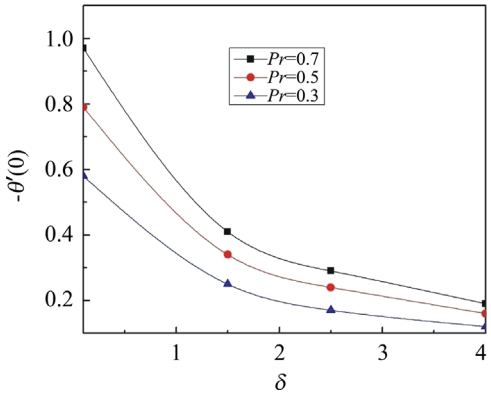

Figure 16 Effects of δ and *Pr* on heat transfer coefficient.

and mass transfer tate is showed in Table 3. The results are found in good agreement. In this paper, numerical solutions will be obtained with the help of the Keller-box method.

Figure 2 shows the effect of the non-linear stretching parameter n and the magnetic parameter M on the dimensionless velocity. It is observed that the dimensionless velocity decreases with increasing values of the non-linear

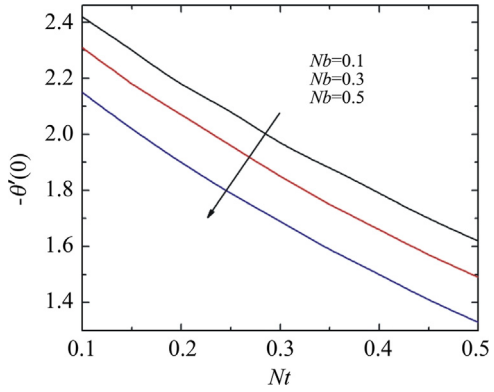

Figure 17 Variation of local Nusselt number $-\theta'(0)$ with Nt for different values of Nb.

Table 1 Comparison of results for skin friction $f''(0)$ when $M = Nb = Nt = \lambda = \delta = 0$, $Le = 1$, $Pr = 6.8$.

N	Hamad et al. [17]	Present study
0.0	0.6283	0.6283
0.2	0.7674	0.7675
0.5	0.8901	0.8901
1.0	1.0004	1.0005
3.0	1.1489	1.1490
10	1.2352	1.2352
20	1.2577	1.2578

Table 2 Comparison of results for $-\theta'(0)$ and $\phi'(0)$ when $Pr = 10$, $n = 10$, $Le = 10$ and $Nt = 0.3$.

$-\theta'(0)$				
Nb	$Ec = 0$		$Ec = 0.1$	
	Hamad [17]	Present study	Hamad [17]	Present study
0.1	3.7716	3.7715	3.6588	3.6588
0.2	3.2515	3.2514	3.1496	3.1496
0.3	2.8279	2.8278	2.7356	2.7356

$\phi'(0)$			
$Ec = 0$		$Ec = 0.1$	
Hamad [17]	Present study	Hamad [17]	Present study
5.6219	5.6212	5.3457	5.3451
0.9981	0.9977	0.8750	0.8746
0.4517	0.4521	0.5250	0.5255

stretching parameter n and the magnetic parameter M. According to the Lorentz force, a retarding body force is introduced by the magnetic field which controverts the direction of the applied magnetic field. By increasing the value of the magnetic parameter M, the retarding body force increases and consequently, the dimensionless velocity decreases. Also, as the magnetic field increases, the boundary layer thickness reduces. Figure 3 exhibits the effects of the non-linear stretching parameter n and the magnetic parameter M on the dimensionless temperature. It is observed that the temperature profile increases with increasing values of the magnetic parameter M. Figure 4 shows that the effect of the magnetic parameter M on the concentration profile. As the magnetic parameter M increases, the nanoparticle concentration also increases. This is due to the Lorentz force which is a resistive force that transverses the fluid motion and therefore, heat is evolved. Hence, for a stronger magnetic field both the thermal boundary layer thickness and the nanoparticle concentration boundary layer thickness become thicker.

Table 3 Calculation table for skin friction coefficient $(-f''(0))$ heat transfer rate $(-\theta'(0))$ and mass transfer rate $(-\phi'(0))$ for various values of magnetic parameter M, velocity slip λ and thermal slip δ when $Pr = 5$, $Nb = Nt = 0.3$, $Le = 2$, $Ec = 0.1$.

M	λ	δ	$-f''(0)$	$-\theta'(0)$	$-\phi'(0)$
0.1	0.2	0.2	0.878734	1.942967	0.759485
0.3	0.2	0.2	0.954825	1.886203	0.741617
0.4	0.2	0.2	0.990667	1.858135	0.731665
0.5	0.2	0.2	1.025242	1.830267	0.721117
1.0	0.3	0.1	1.070591	1.940784	0.919926
1.0	0.4	0.1	0.976827	1.925530	0.946561
1.0	0.5	0.1	0.897480	1.904185	0.963265
1.0	0.1	0.3	1.319597	1.502959	0.447819
1.0	0.1	0.4	1.319597	1.352161	0.320172
1.0	0.1	0.5	1.319597	1.219905	0.208106

Figure 5 shows the effect of the velocity slip parameter ($\lambda = 0.0, 0.1, 0.3, 0.5$) on the velocity profile. It is observed that the dimensionless velocity profile decreases with increasing values of λ. As the velocity slip parameter increases, the slip velocity increases and the fluid velocity decreases. This is because when the slip condition occurs, the velocity of the stretching sheet is not same as the velocity of the flow near the sheet. The effects of variation of the velocity slip parameter on the temperature profile and the concentration profile are presented in Figures 6 and 7. In the presence of a magnetic field and a thermal jump, it is observed that the temperature and concentration profiles increase as the value of the velocity slip parameter λ increases. Figures 8 and 9 exhibit the effects of the thermal slip parameter δ on the dimensionless temperature and nanoparticle volume fraction. It is clearly shown that by increasing the values of δ, the temperature and concentration profiles decrease. As the value of the thermal slip parameter increases, the thermal boundary layer thickness decreases even when a small amount of heat is transferred to the fluid from the sheet.

Figure 10 illustrates the effects of the viscous dissipation parameter (Eckert number) Ec on the dimensionless temperature. It is observed that the temperature increases with increasing values of Ec and that the thermal boundary layer thickness also increases. This is because the rate of heat transfer is decreased at the stretching sheet surface. Figures

11–13 illustrate the effects of the Brownian motion parameter *Nb* and the thermophoresis parameter *Nt* on the dimensionless temperature and concentration, respectively. It is observed that with increasing values of the Brownian motion parameter *Nb*, the temperature profile increases and the concentration profile decreases. Further, we also notice that by increasing the value of the thermophoresis parameter *Nt*, the dimensionless temperature and nanoparticle volume fraction increase. This is due to the fact that the thermophoretic force is produced by the temperature gradient and it creates a very high speed flow away from the stretching sheet. In this way, the fluid is more heated and away from the stretching surface and consequentially, as the thermophoresis parameter *Nt* increases, the thermal boundary layer thickness increases and the temperature gradient at surface decreases as both *Nt* and *Nb* values increase.

Figure 14 depicts the influence of the Lewis number on the dimensionless concentration. It is noticed that the nanoparticle volume fraction experiences a strong reduction for larger *Le* values. The dimensionless Lewis number is defined as the ratio of thermal and mass diffusivity. By increasing the value of *Le*, the thermal boundary layer thickness is increased whereas the concentration boundary layer thickness is reduced. Figure 15 shows that the nature of the skin friction coefficient against the magnetic parameter *M* for increasing values of non-linear stretching parameter *n*. As the non-linear stretching parameter increases, the skin friction coefficient is decreased. This means that fluid motion on the wall of the sheet is accelerated when we strengthen the effects of parameters.

Figure 16 displays the effect of the thermal slip parameter δ against the heat transfer rate for two values of *Pr*. An increase in the Prandtl number, causes the rate of heat transfer to increase. Consequently, it reduces the thickness of the thermal boundary layer. This is due to the Prandtl number, which is defined as the ratio of momentum diffusivity to thermal diffusivity. Fluids with lower Prandtl number will possess higher thermal conductivities and thicker thermal boundary layer structures. So that heat can diffuse from the sheet faster than for higher Pr fluids i.e. thinner boundary layers. Hence Prandtl number can be used to increase the rate of cooling in conducting flows. Figure 17 reveals that the nature of rate of heat transfer against the thermophoresis parameter *Nt* for increasing values of Brownian motion parameter. It is observed that the local Nusselt number is decreased.

5. Conclusions

The boundary layer viscous flow and heat transfer of a nanofluid over a non-linearly stretching sheet with the effect of velocity slip, thermal slip and magnetic field have been studied numerically. The influence of the governing parameters: magnetic parameter *M*, velocity slip parameter λ, thermal slip parameter δ, Eckert number *Ec*, Lewis number *Le*, Brownian motion parameter *Nb*, thermophoresis parameter *Nt*, Prandtl number *Pr*, Non-linear stretching parameter *n* on the velocity, temperature & concentration profiles. It is observed that the present results are equalized with the previous work done by Hamad [17]. The results are as follows:

1. When the magnetic parameter *M* raises, then it reduces the velocity profile, and enhances the temperature and concentration profiles due to the effect of Lorentz force.
2. When the magnetic parameter *M* and the velocity slip parameter are increased individually, then the velocity profile decreases while the temperature and concentration profiles increase.
3. When the velocity slip parameter increases, then it diminishes the velocity profile, and slightly enhances the temperature and concentration profiles.
4. By rising the thermal slip parameter, the temperature and heat transfer rate diminishes when a small amount is heat is transferred to the fluid from the stretching sheet. In the same way the concentration increases and mass transfer reduces.
5. By increasing the thermal slip parameter, the temperature decreases and the concentration increases. Also, the heat and mass transfer reduce.
6. As the value of *Ec* increases, the temperature profile increases.
7. By increasing the Browinian motion parameter *Nb*, the temperature increases and the concentration decreases.
8. By increasing the values of the thermophoresis Parameter *Nt*, the temperature and concentration increase. This is due to the fact that thermophoretic is produced by the temperature gradient. In this case the fluid is more heated and passes away from the stretching sheet.
9. As *Le* increases, the concentration decreases.
10. When the values of *M* and *n* are increased, then the skin friction coefficient also increases.
11. Increasing the Prandtl number *Pr* increases the heat transfer against increasing the thermal slip parameter δ.
12. An increase in the Brownian motion parameter *Nb* decreases the local Nusselt number against increasing the thermophoresis Parameter *Nt*.

Acknowledgement

The authors thank the reviewers for suggesting certain changes to the original paper, for their valuable comments which improved the paper, and for their interest in our work.

References

[1] F.M. Hady, F.S. Ibrahim, S.M. Abdel-Gaied, M.R. Eid, Radiation effect on viscous flow of a nanofluid and heat transfer over a non-linearly stretching sheet, Nanoscale Res. Lett. 7 (2012) 229.

[2] B.C. Sakiadis, Boundary-layer behavior on continuous solid surface, I: boundary-layer equations for two-dimensional and axisymmetric flow, Am. Inst. Chem. Eng. J. 7 (1961) 26–28.
[3] V. Kumaran, G. Ramanaiah, A note on the flow over a stretching sheet, Acta Mech. 116 (1996) 229–233.
[4] R. Cortell, Flow of a viscous fluid over a non-linearly (quadratic) porous stretching surface, in: Proceedings of the International Conference on Future Information Technology and Management Science & Engineering, 2012, pp. 14..
[5] T. Hayat, Z. Abbas, T. Javed, Mixed convection flow of a micropolar fluid over a non-linearly stretching sheet, Phys. Lett. A 372 (2008) 637–647.
[6] M.M. Rashidi, B. Rostami, Nd Freidoonimehr, S. Abbasbandy, Free convective heat and mass transfer for MHD fluid flow over a permeable vertical stretching sheet in the presence of the radiation and buoyancy effects, Ain Shams Eng. J. 5 (3) (2014) 901–912, http://dx.doi.org/10.1016/j.asej.2014.02.007.
[7] K.V. Prasad, K. Vajravelu, P.S. Datti, The effects of variable fluid properties on the hydro-magnetic flow and heat transfer over a non-linearly stretching sheet, Int. J. Therm. Sci. 49 (2010) 603–610.
[8] A. Rapits, C. Perdikis, Viscous flow over a non-linearly stretching sheet in the presence of a chemical reaction and magnetic field, Int. J. Non-Linear Mech. 41 (2006) 527–529.
[9] M. Turkyilmazoglu, Multiple solutions of hydromagnetic permeable flow and heat for viscoelastic fluid, J. Thermophys. Heat. Transf. 25 (4) (2011) 595–605, http://dx.doi.org/10.2514/1.T3749.
[10] Umar Khan, N. Ahmed, S. Irfan, Ullah Khan, S.T. Mohyuddin, Thermo-diffusion effects on MHD stagnation point flow towards a stretching sheet in a nanofluid, Propuls. Power Res. 3 (3) (2014) 151–158.
[11] Md.J. Uddin, W.A. Khan, A.I. Ismail, Lie group snalysis and numerical solutions for magneto convective slip flow along a moving chemically reacting radiating plate in porous media with variable mass diffusivity, Heat. Transf.-Asian Res. (2014), http://dx.doi.org/10.1002/htj.21161.
[12] S.U.S. Choi, Enhancing thermal conductivity of fluids with nanoparticles, ASME International Mechanical Engineering Congress 231/MD 66 (1995) 99–105.
[13] R.S.R. Gorla, S.M.M. El-Kabeir, A.M. Rashad, The boundary layer heat transfer from a stretching sheet circular cylinder in a nano fluid, J. Thermophys. Heat. Transf. 25 (1) (2011) 183–186.
[14] M. Fakour, A. Vahabzadeh, D.D. Ganji, Conducted similar research for a study of heat transfer and flow of nanofluid in permeable channel in the presence of magnetic field, Propuls. Power Res. 4 (2015) 50–62.
[15] O.D. Makinde, A. Aziz, Boundary layer flow of a nanofluid past a stretching sheet with a convective boundary condition, Int. J. Therm. Sci. 50 (2011) 1326–1332.
[16] M. Mustafa, T. Hayat, S. Obaidat, Boundary layer flow of a nanofluid over an exponentially stretching sheet with convective boundary conditions, Int. J. Numer. Methods Heat. fluid Flow. 23 (6) (2013) 945–959.
[17] M.A.A. Hamad, L.K. Mahny, M.R. Abdel-Salam, Similarity solution of viscous flow and heat transfer of nanofluid over a non-linearly stretching sheet, Middle-East J. Sci. Res. 8 (4) (2011) 764–768.
[18] N. Bachok, A. Ishak, I. Pop, Boundary layer stagnation-point flow toward a stretching/shrinking sheet in a nanofluid, ASME J. Heat. Transf. 135 (2013) Article ID: 054501.
[19] K. Zaimi, A. Ishak, I. Pop, Boundary layer flow and heat transfer over a non-linearly permeable stretching/shrinking sheet in a nanofluid, Scientific Reports 4 (2014) Article ID: 4404, http://dx.doi.org/10.1038/srep0440410.1038/srep04404.
[20] F. Aman, A. Ishak, I. Pop, Magnetohydrodynamic stagnation-point flow towards a stretching/shrinking sheet with slip effects, Int. Commun. Heat. Mass Transf. 47 (2013) 68–72.
[21] Md.J. Uddin, O.A. Bég, A. Aziz, A.I.Md Ismail, Group Analysis of free convection flow of a magnetic nanofluid with chemical reaction, Math. Probl. Eng. 2015 (2015) 11 Article ID 621503.
[22] M.J. Uddin, O.A. Bég, N. Amin, Hydromagnetic transport phenomena from a stretching or shrinking non-linear nano material sheet with navier slip and convective heating: a model for bio-nano-materials processing, J. Magn. Magn. Mater. 368 (2014) 252–261.
[23] Md.J. Uddin, O.A. Bég, A.I. Ismail, Radiative convective nanofluid flow past a stretching/shrinking sheet with slip effects, J. Thermophys. Heat. Transf. 29 (3) (2015) 513–523, http://dx.doi.org/10.2514/1.T4372.
[24] Md.J. Uddin, W.A. Khan, A.I. Ismail, G-Jitter Induced magnetohydrodynamics flow of nanofluid with constant convective thermal and solutal boundary conditions, PLoS One 10 (5) (2015) e0122663, http://dx.doi.org/10.1371/journal.pone.0122663.
[25] M.M. Rashidi, N.V. Ganesh, A.K. Abdul Hakeem, B. Ganga, Buoyancy effect on MHD flow of nanofluid over a stretching sheet in the presence of thermal radiation, J. Mol. Liq. 198 (2014) 234–238.
[26] M. Azimi, R. Riazi, Heat transfer of Go-water Nanofluid flow between two parallel disks, Propuls. Power Res. 4 (2015) 23–50.
[27] R.S.R. Gorla, A.J. Chamkha, Natural convective boundary layer flow over a horizontal plate embedded in a porous medium saturated with a non-newtonian nanofluid, Int. J. Microscale Nanoscale Therm. Fluid Transp. Phenom. 2 (2011) 211–227.
[28] A.J. Chamkha, A.M. Aly, MHD free convection flow of a nanofluid past a vertical plate in the presence of heat generation or absorption effects, Chem. Eng. Commun. 198 (2011) 425–441.
[29] A.J. Chamkha, A.M. Aly, H. Al-Mudhaf, Laminar MHD mixed convection flow of a nanofluid along a stretching permeable surface in the presence of heat generation or absorption effects, Int. J. Microscale Nanoscale Therm. Fluid Transp. Phenom. 2 (2011) 51–70.
[30] R.S.R. Gorla, A.J. Chamkha, Natural convective boundary layer flow over a horizontal plate embedded in a porous medium saturated with a nanofluid, J. Mod. Phys. 2 (2011) 62–71.
[31] A.J. Chamkha, A.M. Aly, M.A. Mansour, Similarity Solution for unsteady heat and mass transfer from a stretching surface embedded in a porous medium with suction/injection and chemical reaction effects, Chem. Eng. Commun. 197 (2010) 846–858.

[32] M. Mustaffa, S. Hina, T. Hayat, A. Alsaedi, Slip effects on the peristaltic motion of nanofluid in channel with wall properties, J. Heat. Transf. 135 (4) (2013) 041701.
[33] A. Malvandi, F. Hedayati, D.D. Ganji, Slip effects on unsteady stagnation flow of nanofluid over a stretching sheet, Powder Technol. 253 (2014) 377–384.
[34] U. Khan, N. Ahamed, M. Asadullah, S.T. Mohyuddin, Effects of viscous dissipation and slip velocity on two-dimensional and axisymmetric squeezing flow of cu-water and cu-kerosene nanofluids, Propuls. Power Res. 4 (2015) 40–49.
[35] M. Turkyilmazoglu, Heat and mass transfer of MHD second order slip flow, Comput. Fluids 71 (2013) 426–434.
[36] M. Turkyilmazoglu, Dual and triple solutions for MHD slip flow of non-Newtonian fluid over a shrinking surface, Comput. Fluids 70 (2012) 53–58.
[37] M. Turkyilmazoglu, A note on the correspondence between certain nanofluid flows and standard fluid flows, J. Heat. Transf. 137 (2) (2015) 024501.
[38] M. Turkyilmazoglu, Analytical solutions of single and multi-phase models for the condensation of nanofluid film flow and heat transfer, Eur. J. Mech.-B/Fluids 53 (2015) 272–277.
[39] M.M. Rashidi, B. Rostami, N. Freidoonimehr, S. Abbas-bandy, Free convective heat and mass transfer for MHD fluid flow over a permeable vertical stretching sheet in the presence of the radiation and buoyancy effects, Ain Shams Eng. J. 5 (3) (2014) 901–912.
[40] M.M. Rashidi, E. Erfani, Analytical method for solving steady MHD convective and slip flow due to a rotating disk with viscous dissipation and Ohmic heating, Eng. Comput. 29 (6) (2012) 562–579, http://dx.doi.org/10.1108/02644401211246283.
[41] S. Abbasbandy, T. Hayat, A. Alsaedi, M.M. Rashidi, Numerical and analytical solutions for Falkner-Skan flow of MHD Oldroyd-B fluid, Int. J. Numer. Methods Heat. Fluid Flow. 24 (2) (2014) 390–401.
[42] A.V. Kuznetsov, D.A. Nield, Natural convective boundary-layer flow of a nanofluid past a vertical plate, Int. J. Therm. Sci. 49 (2010) 243–247.
[43] F. Mabood, W.A. Khan, A.I.M. Ismail, MHD boundary layer flow and heat transfer of nanofluids over on linear stretching sheet: a numerical study, J. Magn. Magn. Mater. 374 (2015) 569–576.
[44] S. Mukhopadhyay, Slip effects on MHD boundary layer flow over an exponentially stretching sheet with suction/blowing and thermal radiation, Ain Shams Eng. J. 4 (2013) 485–491.
[45] H.B. Keller, A new difference scheme for parabolic problems, in: B. Hubbard (Ed.), Numerical Solutions of Partial Differential Equations, II, Academic Press, New York, 1971, pp. 327–350.
[46] T. Cebeci, P. Pradshaw, Physical and Computational Aspects of Convective Heat Transfer, Springer, New York, 1998.